IJME

SHEAR STRENGTH CHARACTERISTICS OF WEATHERED JOINTED KENNY HILL INTERBEDDED FORMATION FOR CYLINDRICAL SPECIMEN UNDER DIRECT SHEAR TEST

Hasan Ali Abbas[*]
Department of Building and Construction Techniques Engineering,
Madenat Alelem University College, 10006, Baghdad, IRAQ
Email: hassan_2007a@yahoo.com

Zainab Mohamed
Faculty of Civil Engineering,
Universiti Teknologi MARA, 40450 Shah Alam, Selangor, MALAYSIA

Muntadher J. Taher
Faculty Member of Civil Engineering,
University of Warith Al-Anbiyaa, 56001, Karbala, IRAQ

Sakhiah Abdul Kudus
Faculty of Civil Engineering,
Universiti Teknologi MARA, 40450 Shah Alam, Selangor, MALAYSIA

Manaf Raid Salman and Hasanain Muhammad Ghaltan
Department of Building and Construction Techniques Engineering,
Madenat Alelem University College, 10006, Baghdad, IRAQ

The sliding failures commonly occur in interbedded formations along the weakness plane of the bedding plane a sedimentary rock or the joint interface. Therefore, studying the shear strength characteristics at the bedding plane or interface is crucial for evaluating the expected failure plane. In this study, the shear strength characteristics of planar jointed Kenny Hill shale, sandstone, and shale-sandstone specimens were investigated using the direct shear box method. The results reveal that the friction angle values for the planar sandstone, shale-sandstone, and shale are *31.28°*, *21.1°*, and *19.34°*, respectively. These findings, combined with the shear stress-strain behavior, suggest that the interface (shale-sandstone) is primarily influenced by the shale characteristics rather than the sandstone characteristics. Hence, it is important to consider failure along the interface when analyzing critical conditions, particularly in slope failure scenarios.

Key words: shear strength, planner joint, direct shear, weathered sandstone, weathered shale, interbedded.

1. Introduction

Interbedded sedimentary formations are prone to slope failures primarily due to the presence of weakness planes along the lithologies (i.e., joint interfaces) or bedding planes of the sedimentary rock mass [1]; [2]. The neglectable tensile strength is the critical characteristics of these discontinuities [3]. Shear strength is a crucial input parameter in the analysis of slope failure [4], particularly regarding the shear strength at joint interfaces within interbedded formations or within the rock mass itself. The Kenny Hill interbedded formation

---

[*] To whom correspondence should be addressed

primarily consists of two lithologies: weathered sandstone and shale, known geologically as quartzite and phyllite, respectively [5-10]. Sandstone is characterized as a gritty, massive rock material with high strength under point loading and medium strength under punch loading [6];[11]. In contrast, shale is recognized as a soft, weak rock [12] with an evident anisotropic behavior [13-15].

Several previous studies have investigated the geology of the rock mass and mechanical properties of the interbedded Kenny Hill formation, considering either a single or composite rock material. Mohamed [16] grouped the Kenny Hill formation into four categories based on the weathering grades of the formation layers. These layers can vary in weathering grade from highly to slightly weathered shale and sandstone. The weathered phyllite (shale) in the Kenny Hill formation are identified by four categories, which exhibit varying interbedded ratios and frequencies within the massive sandstone lithology, as explained in [5]; [17]. The dip of the bedding can be formed at various angles between shale and sandstone [18].

A new geological classification system for the Kenny Hill formation was developed by Mohamed *et al.* [7] based on studies of local outcrops [19];[20] and a standard classification [21]. The durability of shale against tropical weather conditions was studied by Mohamed [22], who monitored the swelling and shrinkage of shale rock material. The findings of this study align with the results of [23] and [7], which suggest that this type of rock material exhibits high sensitivity to moisture content [24] and sampling disturbance [25]. These observations highlight the impact of tropical weather on interbedded formation failure, such as open cut collapses and ground heaving. The rock mass resistivity of phyllite and quartzite was characterized Awang *et al.* [26]. The range of resistivity values indicates that resistivity tends to increase as the weathering grade declines. Specifically, phyllite resistivity ranges from *30* to *1200* Ohm-m, while quartzite resistivity ranges from *600* to over *5000* Ohm-m, depending on the weathering grade.

The physical properties of shale and sandstone were presented by Mohamed Z. *et al.* [18]. The values of slaking durability, rebound hammer, and dry density of sandstone were noticeably higher than those of shale, and these values tended to increase as the degree of rock material weathering decreased. Furthermore, Awang *et. al.* [26] observed that porosity increased with the degree of weathering, while density significantly decreased. In a study by Mohamed Z. *et al.* [18], thin sections were examined for various weathering grades of sandstone and shale. The matrix percentage tended to increase with the degree of weathering. However, the weathered shale structure exhibited a higher percentage of the matrix compared to the weathered sandstone, resulting in a smoother texture for shale.

The engineering properties of weathered shale and sandstone were presented by Mohamed [27]. The uniaxial compressive strength of weathered shale ranged between *3.5 MPa* and *11.5 MPa*, while moderately weathered sandstone exhibited a range of *35 MPa* to *56 MPa* [12]. The elastic Young's modulus (E_{50}) ranged between *0.12* and *0.9* for shale, and between *4.6* and *7.4* for sandstone. In addition, Mohamed [27] utilized direct shear tests to investigate the shear strength parameters of jointed sandstone and shale specimens with dimensions of *100 mm* x *100 mm* x *50 mm*. The friction angle for jointed sandstone was measured as *28°*, while for jointed shale it was *25.6°*. However, the friction angle between shale and sandstone was not considered, neglecting the possibility of sliding at the interface between the two lithologies. The limited number of specimens used to determine shear strength introduces uncertainty and may lead to a reduction in accuracy.

In this study, the shear strength of five shale specimens, ten sandstone specimens, and five shale-sandstone specimens is investigated using high stiffness direct shear apparatuses with various normal stress applications. The research aims to characterize the shear strength of all potential sliding failures along the planar joints of the Kenny Hill interbedded formation. The Mohr-Coulomb failure criterion is adopted in the analysis of the results to determine the friction angle.

2. Methods and material

Figure 1 shows a geological map of Peninsular Malaysia, highlighting the sampled area of the study. The samples were collected during excavation activities for a slope nailing project and consisted of weathered shale and sandstone blocks. To preserve the natural water content, the blocks were numbered and wrapped in plastic before being transported to the rock mechanics laboratory at UiTM's College of Civil Engineering in Shah Alam, Malaysia, for preparing and testing.
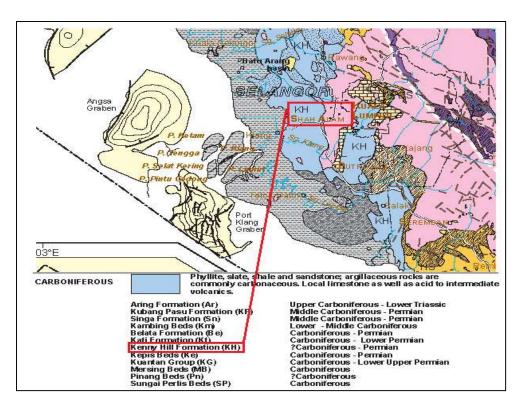
Fig.1. Geological map of Shah Alam and the location of Kenny Hill formation [28].

2.1. Specimens preparation

The shear strength along planar joints of weathered shale, sandstone, and sandstone-shale is determined by applying shearing stress using the direct shear box. Cylindrical specimens with an NX diameter and a height ranging from *50 mm* to *70 mm* are prepared for testing. The shearing face of the specimens is carefully cleaned and smoothed using sandpaper to ensure that no disturbing material remains after specimen preparation.

To facilitate testing, the cylindrical specimens are placed inside a specially designed steel mould with a prismatic shape. This mould consists of upper and lower parts, with a cylindrical hollow in which the cylindrical specimen is placed. The fabrication of this mould enables the direct shear apparatus to effectively test the cylindrical specimens.

2.2. Test apparatus and procedure

2.2.1 Direct shear test

Figure 2 depicts the high stiffness direct shear box equipment, which adheres to the recommended standards of the International Society for Rock Mechanics (ISRM) [29]. The shearing action occurs as a result of the movement of the bottom part of the shear box, while the top part remains fixed. Prior to initiating the shearing process, the normal stress is gradually applied on a spherical surface to prevent the occurrence of bending stresses. The displacement in the normal direction is continuously monitored using a linear variable differential transformer (LVDT), and shearing commences only when no further normal displacement is detected. The shear displacement is recorded by another LVDT, which is positioned parallel to the shearing direction. The shear load is measured using an S-shaped load cell that is installed on the loading frame, also parallel to the shearing direction. Both the load cell and the two LVDTs are connected to a data logger

(KYOWA) of PCD-300A type. This data logger is further connected to a PC equipped with DCS-100A software, enabling real-time monitoring and recording of the experimental data.

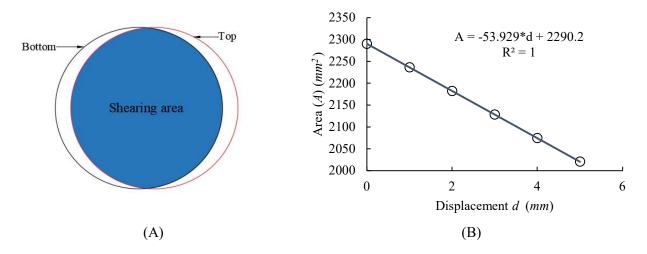Fig.2. Direct shear box equipment component.

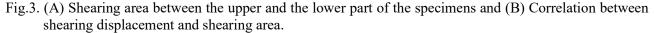### 2.2.2. Correction of shearing and normal stresses

The normal stress and shearing stress are determined by dividing the normal force and shearing force, respectively, by the diametric area of the specimen. As the shearing displacement increases horizontally, the shearing area between the top and bottom specimens changes, requiring simultaneous correction. This ensures accurate measurement of shearing stress and normal stress, as stress is defined as the load applied to a specified area. To precisely measure the shearing stress and normal stress, the shearing area must be determined at each detected shearing load. This is achieved by using AutoCAD 2019 software to calculate the shearing area for every *1 mm* of shearing displacement, as depicted in Fig.3(A).
A correlation is implemented between the shearing displacement and shearing area depending on the area calculated at each *1 mm* displacement [Fig.3(B)].

$$A = -53.929 \cdot d + 2290.2 \tag{2.1}$$

The shearing area can be determined for each shearing displacement using Eq.(2.1), where, (A) is the shearing area $\left(mm^2\right)$ and (d) is the shearing displacement (*mm*). Thus, the shearing stress and normal stress is corrected at each reading by dividing the load to the corrected area.

Fig.3. (A) Shearing area between the upper and the lower part of the specimens and (B) Correlation between shearing displacement and shearing area.

2.2.3. Determination of Shear Strength Parameters

In this study, the Mohr-Coulomb linear criterion was employed as an empirical failure criterion to predict the strength of the rock materials. This criterion is widely used for direct shearing tests and is based on the failure mode of the material. This criterion neglects the intermediate stress σ_2 and assumes that the normal stress σ resultant of two other principal stresses (σ_1 and σ_3) and the shear stress τ are acting on single failure plane [30]. The general mathematical formulation is shown in Eq.(2.2).

$$\tau = c + \sigma\,tan\phi \tag{2.2}$$

where C is the inherent shear strength and ϕ is the internal angle of friction.

3. Results and discussion

3.1. Mechanical properties

Table 1 provides a summary of the mechanical parameters for cylindrical weathered sandstone and shale specimens. The weathered sandstone demonstrated higher values for strength, represented by the uniaxial compressive strength (UCS), as well as for the elastic modulus (E_{50}) and P-velocity (Vp). On the other hand, weathered shale specimens exhibited lower values for Vp, UCS and E_{50}, except for the failure strain value. It is observed that there is a positive relationship between the height of shale specimens and the normal strain induced by normal stress. In other words, as the height of the shale specimen increases, the normal strain that occurs under a given normal stress also increases, which indicates the influence of specimen size on their behavior. This effect is also influenced by the presence of more bedding planes in shale [31]; [32]. This finding suggests that sandstone exhibits higher brittleness compared to shale, as indicated by its higher elastic modulus and failure strain values [18]. This difference could be attributed to the higher grain-to-matrix ratio in sandstone compared to shale, as well as the presence of micro-gaps along the shale bedding [13]; [33].

Table 1. Mechanical properties of weathered sandstone and shale.

Properties	Sandstone	Shale
Vp Pundit (*m/s*)	*4551*	*797*
UCS (*MPa*)	*31.98*	*11.35*
E_{50} (*GPa*)	*0.37*	*0.27*
Failure strain (%)	*2.57*	*4.74*

3.2. Shear strength of weathered sandstone, shale and sandstone-shale

The mechanical properties of the planar joint of sandstone, sandstone-shale, and shale are summarized in Tab.2. It is observed that the friction angles determined from the ultimate shear stress are relatively higher compared to the friction angles determined from the residual shear stress. Additionally, the ultimate and residual friction angles of sandstone are higher than those of both sandstone-shale and shale. On the other hand, the friction angle of sandstone-shale is very close to the friction angle of shale. This suggests that the friction angle in the case of the planar joint between sandstone and shale is primarily controlled by the shale component. These results are not consistent with the findings of Mohamed [27] for planar joints of sandstone, sandstone-shale and shale cubic specimens (Fig.4).

The sandstone friction angle in [27] has a close value to the current study. However, it is worth noting that there is a significant difference in the friction angle values for shale between the two studies, as shown in Fig.4. On the other hand, the friction angle values of [27] indicate no remarkable difference between sandstone, sandstone-shale, and shale friction angle. This might be attributed to the low number of data used to plot the shear strength envelope in comparison with this study.

Table 2. The ultimate and residual friction angle of the planer joints for sandstone, shale and sandstone-shale.

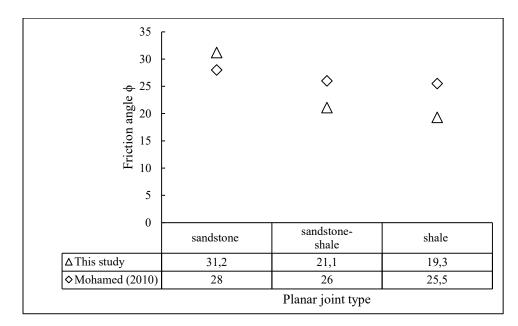| Specimen type	ϕ ultimate	equation	R^2	ϕ residual	equation	R^2
sandstone	*31.28*	$\tau = 0.6077\sigma n$	*0.94*	*29.67*	$\tau = 0.5698\sigma n$	*0.88*
sandstone-shale	*21.1*	$\tau = 0.351\sigma n$	*0.87*	*17.45*	$\tau = 0.3144\sigma n$	*0.94*
shale	*19.34*	$\tau = 0.3857\sigma n$	*0.9*	*14.43*	$\tau = 0.3541\sigma n$	*0.9*

Fig.4. Comparison of friction angles obtained in this study and Mohamed [27] for sandstone, sandstone-shale, and shale.

3.3. Direct shear stress-strain behavior

Figure 5 shows the behavior of sandstone shearing along planar joints. The shear stress-strain curve of sandstone indicates a relatively brittle behavior, with the shearing stress increasing rapidly as the shear strain increases. However, the shear stress-strain curve tends to stabilize after reaching a shear strain of *12%*. The maximum shearing stress value observed was approximately *4.5 MPa* at a normal stress of *7.3 MPa*.
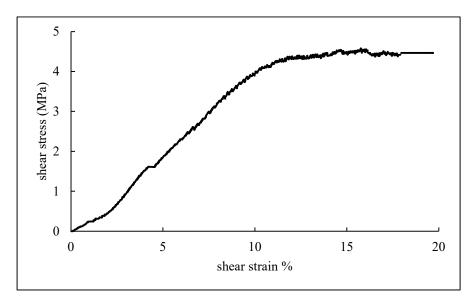

Fig.5. Shear stress-strain curve of sandstone (SS.02) under *16.7 kN* normal load.

Figure 6 illustrates the shearing stress-strain curve of the sandstone-shale planar joint under 4.3 MPa normal stress. The shear stress-strain curve shows a moderately increasing behavior as compared to the sandstone stress-strain behavior. Moreover, the maximum shearing is followed by an obvious decrease of the

shearing stress due to the shale highly worn material at the joint surface as a result of friction. The residual shearing stress is about *2.7 MPa*, meanwhile the maximum shearing stress is *3.4 MPa*.
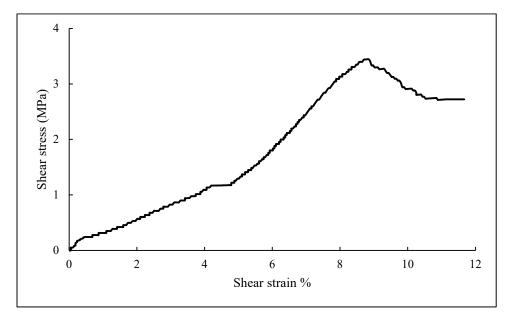

Fig.6. Shear stress-strain curve of sandstone-shale (C02) under *9.9 kN* normal load.

The shale shearing stress-strain curve along planar joints and parallel to the bedding direction of shale is shown in Fig.7. The shear stress-strain curve of shale indicates a gradual increase in the shearing stress. This is attributable to the very soft rock material (fine particle size) and the worn material on the joint surface. Accordingly, shearing along the planar joint experiences sliding or creeping, leading to a stepladder behavior in the stress-strain curve. The maximum shear stress and residual shear stress for the shale specimen are *1.5 MPa* and *1.3 MPa*, respectively.
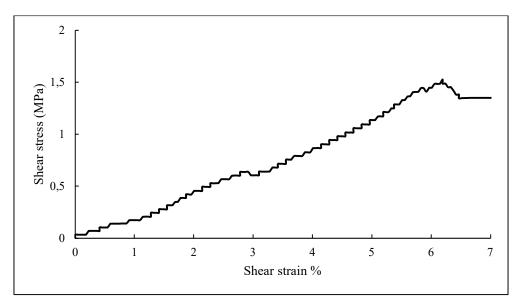

Fig. 7. Shear stress-strain curve of shale (SH.02) under *8.26 kN* normal load.

3.4. Shear strength envelope

Mohr-Coulomb (MC) shear strength envelope was created to recognize the maximum shear stress (τ) regarding the normal stress (σ_n) linear failure criterion [34]. In Eq.(2.2) C and ϕ are the inherent shear strength and the friction angle respectively. However, in the case of planar joints, the shearing load is resisted by only the second term of the equation and the C value can be considered as zero due to the pre-existing shearing plane.

The ultimate and residual shear strength envelopes of sandstone, sandstone-shale, and shale are presented in Fig. 8 and Fig. 9, respectively. These envelopes demonstrate that the shear strength of sandstone is significantly higher than that of sandstone-shale and shale. The shear strength of sandstone exhibits a steep increase as the normal stress grows, resulting in a comparatively sharp inclination of the shear strength envelope. On the other hand, the shear strength of sandstone-shale and shale shows a more gradual increase with increasing normal stress. The envelope for shale represents the lower limit, while the envelope for sandstone-shale falls in between.
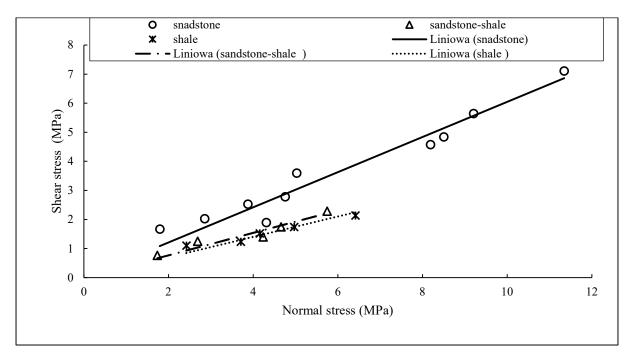

Fig.8. The ultimate shear strength envelope of planed joints for sandstone, shale and sandstone-shale.

However, the shear strength envelope of sandstone-shale was very close to that of shale and had almost the same inclination angle. This indicates that the behavior of sandstone-shale is much similar to shale. Besides, it is evident that the normal stress applied to sandstone is almost double the normal stress applied to shale and sandstone-shale. This is primarily due to the unconfined compressive strength (UCS) of the rock material, where shale exhibits a significant damage if the normal stress exceeds *6 MPa*.
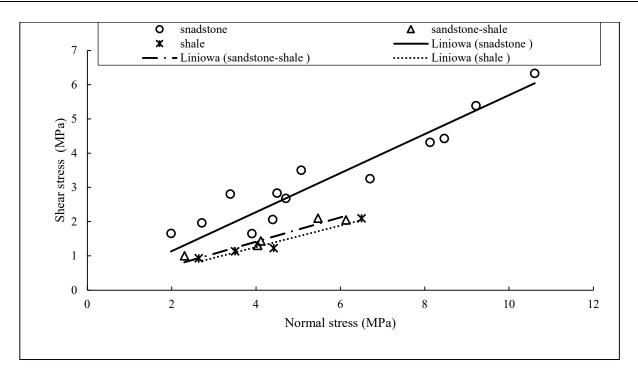
Fig.9. The residual shear strength envelope of planed joints for sandstone, sandstone-shale, and shale.

4. Conclusions

An experimental study was conducted to characterize the shear strength of the planar jointed Kenny Hill interbedded formation. The analysis of the results indicates that the friction angle value is influenced by the roughness of the rock matrix, which is related to the grain size and grain percentage. The following conclusions can be drawn from the study:

1. Under normal conditions, the critical plane of sliding failure is more likely to occur along shale or shale-sandstone planar joints rather than sandstone. This is attributed to the soft rock material of shale compared to the gritty rock material of sandstone.
2. The shear strength characteristics and behavior of shale-sandstone planar joints, as represented by the friction angle value, shear stress-strain curve, and Mohr-Coulomb failure criteria, are predominantly controlled by shale characteristics rather than sandstone characteristics.
3. It is necessary to consider the failure along the interface joint when analyzing the sliding failure of the interbedded formation.

Acknowledgment

References

[1] Eberhardt E., Thuro K. and Luginbuehl M.(2005): *Slope instability mechanisms in dipping interbedded conglomerates and weathered marls – the 1999 Rufi landslide, Switzerland.*– Eng. Geol., vol.77, No.1-2, pp.35-56, https://doi.org/10.1016/j.enggeo.2004.08.004.

[2] Yue Z. and Lee C. (2002): *A plane slide that occurred during construction of a national expressway in Chongqing, SW China.–* Q. J. Eng. Geol. Hydrogeol., vol.35, No.4, pp.309-316, https://doi.org/10.1144/1470-9236/01004.

[3] Priest S.D. (1993): *Discontinuity Analysis for Rock Engineering.–* Springer, Dordrecht,

[4] Stead D. and Wolter A.(2015): *A critical review of rock slope failure mechanisms: the importance of structural geology.–* J. Struct. Geol., vol.74, pp.1-23, https://doi.org/10.1016/j.jsg.2015.02.002.

[5] Roslan N. (2017): *The Potential Susceptibility of Urban Hardrock Aquifers to Hydraulic and Contaminant Stresses: The Case of Shah Alam, Malaysia.–* University of Birmingham, Malaysia.

[6] Mohamed Z., Mohamed Kamaruzzaman and Haryati Awang (2007): *Empirical strength models, elastic modulus and stiffness of weathered sandstone and shale as a composite rock.–* Electron J. Geotech. Eng., vol.12, pp.730.

[7] Mohamed Z., Rafek Abd Ghani and Ibrahim K. (2006): *A geotechnical engineering characterisation of interbedded Kenny Hill weak rock in Malaysian wet tropical environment.–* Electron J. Geotech. Eng., vol.11C, pp.662.

[8] Ho L. (1995): *Some engineering geology characteristics of the Kenny Hill Formation, Kuala Lumpur.–* Bull. Geol. Soc. Malaysia, vol.21, No.1, pp.9-11.

[9] Tan B. and Yeap E. (1977): *Structure of the Kenny Hill Formation, Kuala Lumpur and Selangor.–* Geol. Soc. Malaysia, Bull, vol.8, pp.127-129.

[10] Gue S. and Muhinder S. (2000): *Design & Construction of A LRT Tunnel in Kuala Lumpur.–* Seminar on Design, Construction, Operation and Other Aspect of Tunnel, International Tunnelling Association & The Institution of Engineers, vol.1, pp.1-5. https://gnpgroup.com.my/wp-content/uploads/2017/03/2000_01.pdf.

[11] Alhamwi H.A.A. (2020): *Anisotropic Behavior and Deformation of Composite Weathered Sandstone and Shale Under Destructive and Non-Destructive Stresses.–* PhD thesis, Universiti Teknologi MARA, Malaysia.

[12] Mohamed Z., Mohamed K. and Cho G.C. (2008): *Uniaxial compressive strength of composite rock material with respect to shale thickness ratio and moisture content.–* Electron J. Geotech. Eng., vol.13, pp.1-10.

[13] Abbas H.A., Mohamed Z. and Mohd-Nordin M.M. (2022): *Characterization of the body wave anisotropy of an interbedded sandstone-shale at multi orientations and interlayer ratios.–* Geotech. Geol. Eng., vol.40, pp.1-17, https://doi.org/10.1007/s10706-022-02096-8.

[14] Abbas H.A. and Mohamed Z. (2020): *Anisotropic index strength behaviour and failure mode validation of weathered shale.–* Geomech. Geoengin., vol.17, No.2, pp.1-19, https://doi.org/10.1080/17486025.2020.1839676.

[15] Abbas H.A., Mohamed Z. and Kudus S.A. (2023): *Anisotropic AE attenuation in mapping of composite specimen progressive failure under unconfined loading.–* Int. J. Geomech., vol.23, No.4, pp.04023005, https://doi.org/10.1061/IJGNAI.GMENG-7940.

[16] Mohamed Z. (2004): *Engineering Characterization of Weathered Sedimentary Rock for Engineering work.–* National University of Malaysia, Malaysia.

[17] Musbah A.W. (1980): *Keratan stratigrafi Formasi Bukit Kenny di Bukit Pantai, Kuala Lumpur.–* Sains Malaysiana, vol.9, pp.1-10.

[18] Mohamed Z., Rafek Abd Ghani and Ibrahim K. (2007): *Characterisation and classification of the physical deterioration of tropically weathered kenny hill rock for civil works.–* Electron J. Geotech. Eng., vol.12, pp.16.

[19] Santi P.M. and Higgins J.D. (1998): *Methods for predicting shale durability in the field.–* Geotech. Test. J., vol.21, No.3, pp.195-202.

[20] Komoo I. (1988): *Physical characterization of weathering profile of clastic metasediments of Peninsular Malaysia.–* Proc. of the 2nd Int. Conf. on Geomechanics in Tropical Soils, vol.1, pp.37-42.

[21] BS5930. (1999): *Code of practice for site investigations.–* London.

[22] Mohamed Z. (2007): *Soft rock geo-characterization technique and its significant behavior in tropical climate.–* Electron J. Geotech. Eng., vol.12, pp.1-10.

[23] Brown E., Fairhurst Ch. and Hudson J.A. (1993*): Comprehensive Rock Engineering-Principles, Practice and Projects. Volume 3: Rock Testing and Site Characterization.–* Pergamon Press, London.

[24] Mohamad E., Komoo I., Kassim K.A. and Gofar N. (2008): *Influence of moisture content on the strength of weathered sandstone.–* Malays. J. Civ. Eng., vol.20, No.1, pp.137-144, https://doi.org/10.11113/mjce.v20.15762.

[25] Kanji M. (2014): *Critical issues in soft rocks.–* J. Rock Mech. Geotech. Eng., vol.6, No.3, pp.186-195, https://doi.org/10.1016/j.jrmge.2014.04.002.

[26] Awang H., Mohamed Z. and Nawawi M. (2008): *Using resistivity imaging technique to characterize interbedded weathered sedimentary rock mass.*– Symposium on the Application of Geophysics to Engineering and Environmental Problems Proceedings, vol.2008, pp.1159-1165, https://doi.org/10.4133/1.2963225.

[27] Mohamed K. (2010): *Bearing Capacity of Interbedded Weak Weathered Sedimentary Rock.*– Universiti Teknologi MARA, Malaysia

[28] Tate R., Tan D. and Ng T. (2008): *Geological map of peninsular Malaysia.*– Geological Society of Malaysia & University Malaya, Malaysia.

[29] Muralha J., Grasselli G., Tatone B., Blümel M., Chryssanthakis P. and Yujing J. (2014): *ISRM suggested method for laboratory determination of the shear strength of rock joints: revised version.*– Rock Mech. Rock Eng., vol.47, No.1, pp.291-302, https://doi.org/10.1007/s00603-013-0519-z.

[30] Jaeger J.C. and Cook. N.H. (1979): *Fundamentals of Rock Mechanics.*– Chapman and Hall, London.

[31] Thuro K., Plinninger R., Zäh S. and Schütz S. (2001): *Scale effects in rock strength properties. Part 1: Unconfined compressive test and Brazilian test.*– Eurock 2001; Rock mechanics, a challenge for society, vol.1, pp.169-174.

[32] Tuncay E. and Hasancebi N. (2009): *The effect of length to diameter ratio of test specimens on the uniaxial compressive strength of rock.*– Bull. Eng. Geol. Environ., vol.68, No.4, pp.491, https://doi.org/10.1007/s10064-009-0227-9.

[33] Abbass H., Mohamed Z. and Yasir S. (2018): *A review of methods, techniques and approaches on investigation of rock anisotropy.*– AIP Conf. Proc., vol.2020, No.1, pp.020012, https://doi.org/10.1063/1.5062638.

[34] Labuz J. and Zang A. (2012): *Mohr-Coulomb failure criterion.*– Rock Mech. Rock Eng., vol.45, No.6, pp.975-979, https://doi.org/10.1007/s00603-012-0281-7.